CONF-830702--9

DE83 009535

HYDRODYNAMIC STABILITY OF INVERTED ANNULAR FLOW IN AN ADIABTIC SIMULATION

G. De Jarlais, M. Ishii and J. Linehan*

Reactor Analysis and Safety Division
Argonne National Laboratory
9700 South Cass Avenue
Argonne, IL 60439

ABSTRACT

In experiments, inverted annular flow was simulated adiabatically with turbulent water jets, issuing downward from long aspect nozzles, enclosed in gas annuli. Velocities, diameters, and gas species were varied, and core jet length, shape, break-up mode, and dispersed-core droplet sizes were recorded at approximately 750 data points. Inverted annular flow was observed to develop into inverted slug flow at low relative velocities, and into dispersed droplet flow at high relative velocities.

For both of the above transitions from inverted annular flow, a correlation for core jet length was developed by extending work done on free liquid jets to include this new, coaxial, jet disintegration phenomenon. The result, showing length dependence upon diameter, jet Reynolds number, jet Weber number, void fraction, and gas Weber number, correlates the data well, especially at moderate-to-large relative velocities.

Correlations for core shape, break-up mechanisms and dispersed core droplet size for the case of transition to inverted slug flow were developed by again extending free jet work, while similar correlations for the case of transition to dispersed droplet flow were developed by extending roll wave entrainment studies.

*Department of Mechanical Engineering, Marquette University, 1515 W. Wisconsin Avenue, Milwaukee, WI 53233.

DISCLAIMER

NOMENCLATURE

d	Jet diameter
d_{10}	Linear mean droplet diameter
d_{30}	Volume/surface area mean droplet diameter
d_h	Hydraulic equivalent diameter of flow passage
d_{max}	Average maximum droplet diameter
g	Gravity acceleration
j_G	Gas volumetric flux (superficial velocity)
j_J	Liquid jet volumetric flux (superficial velocity)
K	Constants, used in Eqs. (27), (28), (31), (35)
L	Jet break-up length
m	Constants, used in Eqs. (27), (28), (29), (31), (35)
$N_{\mu F}$	Liquid viscosity number, defined by Eq. (39)
$N_{\mu G}$	Gas viscosity number, defined by Eq. (47)
$N_{\mu J}$	Liquid jet viscosity number ($= \sqrt{We_J}/Re_J$)
Re_J	Liquid jet Reynolds number ($= \rho_J v_{rel} d/\mu_J$)
$Re_{G,rel}$	Gas Reynolds number ($= \rho_G v_{rel} d_h/\mu_G$)
v_G	Gas velocity
v_J	Liquid jet velocity
v_{rel}	Relative velocity ($= \lvert v_G - v_J \rvert$)
We_d	Droplet Weber number defined by Eq. (44)
We_G	Gas Weber number, free jet ($= \rho_G v_J^2 d/\sigma$)
$We_{G,rel}$	Gas Weber number ($= \rho_G v_{rel}^2 d/\sigma$)
We_J	Liquid jet Weber number ($= \rho_J v_J^2 d/\sigma$)
$We_{J,rel}$	Liquid jet Weber number ($= \rho_J v_{rel}^2 d/\sigma$)
X	Parameter defined by Eq. (29)

Greek Symbols

α	Void fraction
δ	Initial disturbance
$\Delta\rho$	Density difference ($= \rho_J - \rho_G$ or $= \rho_F - \rho_G$)
λ	Wavelength of maximum growth rate
μ_F	Liquid viscosity
μ_G	Gas viscosity
μ_J	Liquid jet viscosity
ρ_F	Liquid density
ρ_G	Gas density
ρ_J	Liquid jet density
σ	Surface tension

Subscripts

d	Droplet
I	Transition from laminar to turbulent
II	Transition from varicose to sinuous
III	Transition from varicose or sinuous to atomization or roll wave entrainment
F	Liquid
G	Gas
J	Liquid jet
rel	Relative

INTRODUCTION

Inverted annular flow is important in the areas of LWR accident analysis, cryogenic heat transfer, and other confined, low quality film boiling applications. And yet, while many analytical and experimental studies of heat transfer in this regime have been performed, there is very little understanding of the basic hydrodynamics of inverted annular flow. As a result, many film boiling applications are amenable to only limited analysis at present. One example of this can be seen in large-scale LWR safety codes such as TRAC and RELAP, which are essentially constrained by the not-well understood two-phase thermohydraulics under various accident conditions, including those resulting in inverted annular flow.

Inverted annular flow can be visualized as a liquid jet-like core surrounded by a vapor annulus. The shape of the liquid/vapor interface, the stability of the liquid jet core, and the disintegration/entrainment of this liquid core must be understood, and predictive methods established, in order to clarify the modeling of this regime and the development of interfacial transfer correlations. In typical film boiling experiments, however, control and measurement of the flow parameters necessary for such an understanding is difficult, if not impossible, to achieve. The principle objective of this study, therefore, is to systematically investigate the effect of various flow parameters on the jet core hydrodynamics, by means of an adiabatic simulation of inverted annular flow. Such a simulation, unlike actual film boiling, allows ready establishment of specific velocities, geometries, and fluid properties.

In addition to this experimental investigation, the hydrodynamics of free jets has been reviewed in this study. In light of our experimental results, there may be many similarities between free jet behavior and the behavior of the liquid core in inverted annular flow.

REVIEW OF FREE JET LITERATURE

Since inverted annular flow may be viewed as having a liquid jet in its core, jet disintegration mechanisms are reviewed here in detail. Most of the existing analytical works and experimental data are on the free liquid jet disintegration in stagnant gas phase. It is obvious that there exist significant differences between the free jet and inverted annular flow. The inverted annular flow is co-axial jets of liquid and vapor, therefore, the pressure and shear force from the outer vapor jet can strongly influence the stability of the liquid jet, as can the presence of a solid boundary. Nevertheless, the existing studies on free jet break-up give significant insight to inverted annular flow behavior.

For free jets, jet character and break-up have often been represented on curves of jet length divided by jet diameter versus jet velocity, as in Fig. 1 and Fig. 2. Three different break-up mechanisms have been identified, with distinctions also made between laminar and turbulent jets. In Fig. 1, the region labled AB represents the varicose break-up of a laminar jet. This axisymmetric break-up region is the only one which may be treated, in great detail, analytically. Weber [1] showed that for a viscous jet in a vacuum, jet length can be expressed as

$$L/d = \ell n[d/2\delta][1 + 3\ N_{\mu J}]\sqrt{We_J} \qquad (1)$$

where δ is the initial disturbance of the jet's surface. For most laminar jets, the term $\ell n[d/2\delta]$ proves to be about 12. In this laminar, varicose region, Rayleigh [2] predicted a maximum growth rate for the wavelength

$$\lambda = 4.51\ d \qquad (2)$$

while Weber [1], including the effect of viscosity, showed that the maximum growth rate is for

$$\lambda = \pi \sqrt{2} [1 + 3 N_{\mu J}]^{1/2} d \tag{3}$$

And Lafrance [3] predicted the size of smaller, satellite drops appearing between main drops formed at break-up, using non-linear analysis.

Experiments by many researchers have produced results in general agreement with the analytical solutions for this region, for various fluids, nozzles and ambient atmospheres. Even for liquid jets into liquid mediums, λ/d has proven to be between 4.5 and 7 [4]. Tyler and Watkin [5] developed an empirical length correlation showing a viscosity dependence opposite that of Weber,

$$L/d = 10 \left[1 + \frac{1}{4100} N_{\mu J}^{-1.5}\right] \sqrt{We_J} \tag{4}$$

but this may represent the effect of viscosity on initial disturbance levels [6] or velocity profile development [7]. Grant and Middleman [6] developed empirical correlations to modify Weber's theory

$$L/d = \ell n(d/2\delta)[(1 + 3 N_{\mu J}) \sqrt{We_J}]^{0.85} \tag{5}$$

and to express the initial disturbance as

$$\ell n(d/2\delta) = -2.66 \ell n N_{\mu J} + 7.68 \tag{6}$$

Phinney [8] developed similar $\ell n(d/2\delta)$ correlations. And many investigators, including Fenn and Middleman [9], noted that various ambient atmospheres have no affect on varicose break-up behavior.

In Fig. 1, point I is the transition from laminar to turbulent jet behavior, first identified by Smith and Moss [10]. For long aspect nozzles, turbulence occurs at $Re_J \triangleq 2300$, since fully developed pipe flow is present. For laminar flow from long aspect nozzles, turbulence can result from velocity profile relaxation [7] with its attendant energy redistribution. Orifice nozzles with rough surfaces, industrial surfaces or turbulence in their feed lines can also produce turbulent jets [11]. Feed line turbulence may explain why some sharp-edged orifices show a transition like point I [12], while others do not [13]. Outflow conditions for sharp-edged orifices were investigated in detail by Iciek [14]. For long tubes Grant and Middleman [6], also using the data of Tyler and Richardson [15], developed the empirical correlation

$$Re_{J,I} = 325\ N_{\mu J}^{-0.28} \tag{7}$$

while Phinney [19], also using long tube nozzles, developed the empirical correlation

$$We_{J,I} = 625 \tag{8}$$

Confusion over this transition has been extensive because of the various causes of turbulence mentioned above. In addition, this transition may be confused with the transition labeled II on Fig. 1 and Fig. 2, denoting the change from varicose to sinuous, asymmetric break-up, which will be discussed

in detail later. Both may result in a maximum in the L/d vs. v_J curve, the onset of turbulence may also mark the onset of sinuous behavior, and a turbulent varicose jet may appear somewhat sinuous, since macroscale turbulence will prevent the jet from being truly axisymmetric.

Region CD in Fig. 1 represents the varicose break-up of a turbulent jet, where a great deal of conflicting empirical correlations have been developed. Grant and Middleman [6] and Iciek [16] developed similar correlations

$$L/d = 8.51\ We_J^{0.32} \tag{9}$$

and

$$L/d = 11.5\ We_J^{0.31} \tag{10}$$

respectively. Miesse [11], expanding on Baron's work [17], developed a correlation of the form

$$L/d = 540\sqrt{We_J}\ Re_J^{-.625} \tag{11}$$

while Chen and Davis [12], Phinney [18] and van de Sande and Smith [19] published correlations of the form

$$L/d = \ell n(d/2\delta)\sqrt{We_J} \tag{12}$$

with attendant correlations for $\ell n(d/2\delta)$, often approximated by a constant value of 4 [18,19]. Chen and Davis also give data on the amplitude of surface

disturbances and mean droplet sizes. This latter data includes the effect of satellite droplets, but still indicates a maximum growth rate for the wavelength in the general range of

$$2.25\ d < \lambda < 20\ d \tag{13}$$

while most of the data from Miesse [11] is in the range of

$$2\ d < \lambda < 12\ d \tag{14}$$

Point II in Fig. 1 and Fig. 2 is the transition to drag-induced break-up, marked by the appearance of sinuous, assymetric waves. Weber [1] hypothesized, that for a laminar jet, this transition would occur when aerodynamic pressure effects become important, at approximately $We_G = 2.0$ for air/water [9], where We_G is based on ambient density. In experiments, Fenn and Middleman [9] found the transition for laminar jets to be at

$$We_{G,II} = 5.3 \tag{15}$$

For turbulent jets, Iciek [16] found the transition to sinuous break-up to occur at

$$We_{G,II} = 1.2 \tag{16}$$

Ohnesorge [20], ignoring the effect of ambient density, developed the empirical correlation

$$Re_{J,II} = 53\ N_{\mu J}^{-3/4} \tag{17}$$

but, like Eq. (7), this may actually represent the transition from laminar to turbulent jet flow.

Point III in Fig. 2 is the transition to atomization or secondary drag-induced break-up. Littaye [22] showed that by assuming atomization occurs when drag exceeds inertia by a certain factor, We_G = const. would be the transition criteria, with the constant to be determined experimentally. Miesse [11] found that his data for turbulent jets into air indicated a transition to atomization at

$$We_{G,III} = 6.35 \tag{18}$$

Ohnesorge [20], again ignoring the effect of ambient density, developed the empirical correlation for atomization inception

$$Re_{J,III} = 300\ N_{\mu J}^{-3/4} \tag{19}$$

which is in substantial agreement with Merrington and Richardson [23] data for low viscosity liquids into an air atmosphere. As in the case of transition to sinuous behavior, it might be expected that laminar jets will require higher velocities than turbulent jets for inception of atomization.

Region E in Fig. 1 and Fig. 2 is the region of sinuous break-up and atomization, shown as a dotted line in Fig. 1 because even general trends in jet length for this region are disputed. Levich's [24] calculation shows that, in the absence of interaction with the ambient medium, sinuous jet length increases linearly with velocity. Tanazawa and Toyoda [25] claim that L/d continually increases with v_J.

However, Merrington and Richardson [23] point out that interfacial resistance will rapidly decrease break-up times, as their data (some of it for jets issuing from aircraft) indicates. Fenn and Middleman [9] have defined drag-induced break-up as the point where L/d rapidly decreases with v_J, due to interfacial loading. Lienhard and Day [26] have correlated their data for drag-induced break-up as

$$L/d = 2.75 \times 10^{10} \sqrt{We_J}\, Re_J^{-2} \tag{20}$$

which shows L/d inversely proportional to velocity.

Finally, Kusui [27] proposes that after an initial decrease in length with velocity, a constant value of L/d is maintained, while Ivanov [28] suggests that after the start of drag-induced break-up, jet length may first decrease, then increase, and finally decrease again.

These widely divergent results may be a matter of different definitions of jet length, since atomization creates a liquid core much more complicated and poorly defined than the original jet issuing from the nozzle. Defining jet length as the distance from the nozzle at which point a continuous thread of liquid is no longer present for a significant percentage of the time, it may be impossible to ascertain jet length optically. Using a conductance probe [18,27] such a jet length can be determined, but at this distance from the nozzle mean liquid momentum and surface area per unit volume are radically different than that of the original jet. In contrast, one might define jet length as the distance at which surface area of the jet increases rapidly, which might yield significantly shorter lengths.

Droplet size in the atomization regime is not well understood. Merrington and Richardson [23] developed an empirical dimensional correlation for the linear mean diameter

$$d_{10} = 500(\mu_J/\rho_J)^{1/5}\, v_{rel}^{-1} \tag{21}$$

for stationary and aircraft-mounted jets, where v_{rel} is the relative velocity between liquid and gas. Working with air blast atomizers, in which liquid jets are discharged into high velocity gas streams, Nukiyama and Tanaszwa [29] developed an empirical, dimensional correlation for the volume/surface area mean diameter

$$d_{30} = \frac{585}{v_{rel}}\left(\frac{\sigma}{\rho_J}\right)^{0.5} + 597\left(\frac{\mu_J}{\sqrt{\sigma\rho_J}}\right)\left(1000\,\frac{j_J}{j_G}\right) \tag{22}$$

where j_J/j_G is the ratio of liquid and gas volume flow rates, d_{30} is in microns, v_{rel} is in m/sec, and σ, ρ_J and μ_J are in c.g.s. units. Various liquids were used in their experiments, with air used exclusively for the gas flow.

CONFINED, COAXIAL JETS

Unlike free, liquid jets, very little is known about confined, coaxial liquid and gas jets. Using numerical methods, Jensen [30] generated curves of wavelength and jet length as a function of void fraction, liquid velocity, gas density, and Weber number based on liquid density and relative velocity, for a confined water/steam system. However, his analysis was limited to plane, rather than cylindrical, jets, in laminar, varicose break-up only. His results for wavelength show a range of approximately

$$1\,d < \lambda < 15\,d \tag{23}$$

with λ decreasing with increasing values of $We_{J,rel}$, and increasing with increasing void fraction. His results for jet length are extended out to v_{rel}

values of up to 12 m/s, which, in light of free jet literature and the experiments reported on later in this paper, would indicate actual conditions far removed from varicose break-up. However, the general trends from Jensen's curves are interesting, showing the effect of Kelvin-Helmholtz instability on accelerating varicose break-up of jets when in confined geometries. In rough approximation, these curves show that

$$L/d \sim (\rho_G/\rho_J)^{-1.3} (\alpha)^{1.3} (v_J) (We_{J,rel})^{-1.4} \quad (24)$$

Working with liquid jet gas pumps, in which a high velocity jet entrains a flow of gas, Cunningham and Dopkin [31] found that maximum efficiency was obtained when mixing throat length equaled the break-up length of the atomized jet. Their empirical expression for jet length,

$$L/d = 7.86 \times 10^6 \left(\frac{\alpha}{1-\alpha}\right) \left(\frac{v_G}{v_J}\right) Re_J^{-1} \quad (25)$$

and their observation that increasing gas density decreased gas length, are interesting. However, for a liquid jet gas pump, v_G is not an independent variable. Rather, v_G is a function of geometry, and jet break-up characteristics. This prevents Eq. (25) from being applied directly to other coaxial jet situations, such as inverted annular flow film boiling.

INVERTED ANNULAR FLOW EXPERIMENT

An adiabatic simulation of inverted annular flow was performed, with turbulent water jets enclosed in gas annuli. See Fig. 3 for a schematic diagram of the test system. The water jets issued from long aspect nozzles made of thin-walled stainless steel tubing. To simulate inverted annular flow conditions, these nozzles were coaxially centered within pyrex tubing, and gas

was introduced through the gap between the stainless steel and the pyrex. Parameters varied in the experiment included jet velocity, jet diameter, gas velocity, gas annulus outer diameter, and gas species. The series of tests performed are summarized in the following table:

Test Series	Nozzle Diameter (cm)	Nozzle Length (cm)	Annulus Outer Diameter (cm)	Initial Void Fraction	Gas Species
A7	0.425	41.	1.66	0.934	Nitrogen
B2	0.763	46.	1.36	0.685	Nitrogen, Helium, Freon-12
B3	0.902	67.	1.36	0.560	Nitrogen, Helium, Freon-12
C1	0.604	37.	0.90	0.549	Nitrogen
C2	0.763	46.	0.90	0.281	Nitrogen

All tests were performed near atmospheric pressure, with flow directed downward. Upward flow was attempted, but the use of low velocity jets, coupled with easy wetting of the pyrex wall (which would not occur in true inverted annular flow) made this impossible. Even with downward-directed flow, wall wetting by entrained droplets at high gas velocities made data acquisition difficult.

Jet break-up lengths were observed visually, with the aid of a strobe light with a 3 μs flash duration. As observed by Chen and Davis [12] and others [4,16], jet length is quite variable, and so a minimum of 100-200 strobe flashes were used to determine an average break-up length at each set of flow conditions, comparable to the 150 exposures Chen and Davis used at each data point for a 5% probability level with a tolerance of three jet diameters. For high gas velocites, a small number of photographs were sometimes used to verify the lengths determined visually, as jet surface roll waves, small droplets and wall wetting made viewing more difficult. Jet length under these conditions was defined as the point at which the

disintegrating jet was continuously wetting the wall, or, when observed, as the point at which the entire core had been deformed into giant, sheet-like segments developing from large amplitude roll waves. This latter type of break-up developed very suddenly, over a very short distance compared to the entire jet core length.

Break-up mechanisms, surface characteristics, and entrained droplets were observed photographically, with a Graphlex 4 x 5 camera using ASA 3000 film and the 3 μs strobe flash for lighting. Jet character could also be determined visually at some flow conditions.

For these large diameter, long aspect nozzles, liquid velocities low enough to prevent well-established turbulent pipe flow would have resulted in severe jet acceleration and thinning due to gravity, with an attendant sharp jump in gas flow area at the nozzle exit. To avoid this, all water jets used in the test series were turbulent, with

$$4300 < Re_J < 33{,}000 \tag{26}$$

Even at these higher velocities, gravity acceleration became significant for some of the longer varicose and sinuous jets. Because of this, velocities and geometries were sometimes adjusted to account for gravity effects. Such adjustments are noted in the following section of this paper, dealing with analysis of the experimental results.

Liquid acceleration adjustments due to interfacial shear were not included in the analysis of data. At varicose and sinuous break-up conditions, the interface, even with macroscale turbulence, was relatively smooth, and gas velocities were moderate, so that shear acceleration was estimated to be at least an order of magnitude less than acceleration due to

gravity. At higher velocities, break-up lengths (and times) decreased drastically as roll waves appeared, so that even shear stresses comparable to those of rough-wavy annular flow [32], while causing acceleration of the same order of magnitude as gravity, would not have time to accelerate the jet core significantly. In addition, jet core diameter and surface smoothness under these high velocity flows were observed to remain relatively constant until very near the break-up point, when large amplitude deformations occurred rapidly.

ANALYSIS OF RESULTS

Analysis of the experimental results was divided into four different areas: jet length, break-up mechanisms, surface characteristics, and dispersed jet core droplet sizes.

1. Jet Length

To correlate jet break-up length, the data was divided into two regions, one in which gas flow conditions had no influence, and a second in which gas flow did have influence. In this first region, the ability of the various correlations for turbulent free jets in varicose break-up (Eqs. (9)-(12)) to correctly correlate the experimental jet length data was tested using linear regression techniques. These free jet correlations were generalized into two basic forms

$$L/d = K_1 \cdot [We_J]^{m_1} \tag{27}$$

and

$$L/d = K_2[Re_J]^{m_2} \sqrt{We_J} \tag{28}$$

Jet diameter and Weber number were adjusted to represent values at 1/2 the break-up time, assuming only gravity acceleration. This adjustment was not large for most of the data, and was made even less important by the form of Eqs. (27) and (28) in which the term

$$d \cdot [\rho_J d v_J^2/\sigma]^m = X \tag{29}$$

appears. Viewing Eq. (29) in light of the continuity equation,

$$d^2 v_J = \text{constant} \tag{30}$$

it becomes apparent that the value of X may be only a weak function of jet acceleration especially at m values approaching 2/3.

Jet Reynolds number was not adjusted to account for acceleration of the jet after leaving the nozzle, because the combining of Eqs. (11) and (12) would suggest that

$$\ln(d/2\delta) = K_2[Re_J]^{m_2} \tag{31}$$

and δ, the initial jet surface disturbance, should be a function of conditions at the exit, rather than at some downstream point.

A best fit of the data was obtained with the following correlation:

$$L/d = 481\ [Re_J]^{-0.5306}\ \sqrt{We_J} \tag{32}$$

which is in general agreement with Miesse's [11] result, Eq. (11), although for a substantially different nozzle design (long aspect tube vs. turbulent

industrial orifice). The data shows a good deal of scatter, with a correlation coefficient of only 0.89.

For the region in which gas flow conditions affected break-up length, another term was added to Eq. (32) to account for this behavior. It was determined, again using linear regression, that the expression

$$L/d = 687\ [Re_J]^{-0.5306}\ \sqrt{We_J}\ [We_{G,rel}/\alpha^2]^{-0.6467} \tag{33}$$

correlated the data very well, with a correlation coefficient of 0.967. In this equation, $We_{G,rel}$, based on gas density and relative velocity, and α were also adjusted to represent values at 1/2 the break-up time. This adjustment was quite small at higher gas velocities.

The term $[We_{G,rel}/\alpha^2]$ may be rewritten as a gas Weber number based upon an effective velocity, v_{rel}/α. This modified velocity term represents the effect of area change due to wave crests on the gas velocity field, and in turn, the reduction in pressure at the wave crest through the Bernoulli principle. It can be seen that for low void fractions and moderate wave amplitude, the velocity of the gas, as it is accelerated over the wave crest, is at least roughly proportional to $1/\alpha$. A more exact expression for the effective relative velocity over the total jet length would be quite complicated, considering that wave amplitude is varying along the jet length, with a growth rate dependent upon relative gas velocity. Extension of Jensen's work [30] would also prove difficult, for a cylindrical geometry and non-varicose break-up, and would be less useful than simple expressions for jet core break-up characteristics.

Jet break-up length data is presented in Figs. 4, 5 and 6, plotted against the correlations given by Eqs. (32) and (33). A total of 741 jet

length observations were made. Some of the data scatter shown by these figures may be due to the difficulties previously mentioned in defining jet length consistently in light of wall wetting. This would explain why jet lengths for A7 trials (initial void fraction =.934) were larger than those for C2 trials (initial void fractions =0.281) in the sinuous and sinuous-roll wave regimes where the jet core could be displaced far from its axis and incur wall contact.

It should be noted that Eq. (33), applied to free jets, would indicate L/d is proportional to $v_J^{0.824}$, a result very similar to that presented by Lienhard and Day [26] in Eq. (20). And Eq. (33) shows trends similar to those calculated by Jensen [30] (Eq. (28)), especially the dependence upon void fraction, even though his calculations were for varicose, laminar plane jets.

The two curves defined by Eqs. (32) and (33) intersect at a value of $[We_{G,rel}/\alpha^2] = 1.73$, and this can be used as the criterion for determining regions of applicability for the two equations.

From the free jet literature, it may be conjectured that, for laminar, confined, coaxial jets, Eqs. (32) and (33) would be replaced by ones of the form

$$L/d = 12\,[1 + 3N_{\mu J}]\,\sqrt{We_J} \tag{34}$$

(see Eq. (1) and text following it) for the region with no dependence upon gas flow, and by

$$L/d = K_3\,[1 + 3N_{\mu J}]\,\sqrt{We_J}\,[We_{G,rel}/\alpha^2]^{m_3} \tag{35}$$

for the region in which gas flow becomes important.

2. Jet Break-up Mechanism

As in free jets, three regimes, or break-up mechanisms were observed for these confined coaxial jets. The first two mechanisms, varicose and sinuous break-up, proved to be the same as those noted for free jets (see Fig. 7). The transition from varicose to sinuous behavior was, however, difficult to define from observations of jet shape, due to large distortions imposed by macroscale turbulence within the water jets. This resulted in many data points being classified as varicose-sinuous or regime-unknown. To resolve this difficulty, the transition point was defined as the region on the jet length curve (Figs. 4, 5 and 6) when interfacial drag, first becomes important, in effect using the same criterion as Fenn and Middleman [9]. This seems appropriate since no clearly varicose jets were observed beyond this point, and only the more turbulent jets appeared somewhat sinuous before this point. From the two jet length correlations developed, Eqs. (32) and (33), the transition criterion is then defined as

$$We_{G,rel,II}/\alpha^2 = 1.73 \tag{36}$$

for these turbulent, coaxial jets. This is comparable to Iciek's [16] value of $We_{G,II} = 1.2$ for turbulent jets, and substantially lower than Fenn and Middleman's value of $We_{G,II} = 5.3$ for laminar jets. This is easily understood, since the rough surface of a turbulent jet should be much more susceptible to interfacial drag than the smooth surface of a laminar jet. As in the case of jet length, the appearance of the term v_{rel}/α, rather than merely the term v_{rel} seen in free jet literature, may be viewed as representing the acceleration of the gas stream as it flows between solid gas annulus wall and the liquid wave crests.

The third mechanism of jet break-up observed in these experiments is that of roll wave entrainment, a more exact, and mechanistically sound description of dispersed droplet formation than the term atomization, used to describe free jet break-up at high relative velocities. Roll waves first appeared on the crests of sinuous waves, while at higher velocities roll waves caused jet break-up before the core exhibited any sinuous behavior. Often a single roll wave developed over a substantial portion of the jet circumference, deforming into a thin, skirt-like sheet. Ligaments or individual droplets could be seen being sheared from the roll wave crests (see Fig. 8). Except at the highest of void fractions, it was not possible to view the entire dispersal of the liquid jet core, due to wall wetting. Because of this, it is possible that after initial core disruption due to large amplitude roll waves, other unobserved dispersion/entrainment mechanisms might also have contributed to droplet formation.

To analyze the data on the inception of roll wave entrainment for this experiment, use was made of roll wave entrainment studies in annular flow. Assuming that entrainment begins when drag force due to high shear gas flow acting on wave crests exceeds the retaining force due to surface tension, Ishii and Grolmes [33] developed entrainment inception criteria for various regimes within annular flow. Their results compare favorably with experimental entrainment studies, including their own limited data. For rough turbulent flow, in which the liquid friction factor is assumed to be independent of liquid Reynolds number, their entrainment inception criterion is

$$\frac{\mu_F \, j_G}{\sigma} \sqrt{\frac{\rho_G}{\rho_F}} \geq N_{\mu F}^{0.8}; \quad \text{for } N_{\mu F} < 1/15 \tag{37}$$

$$\geq 0.1146; \text{ for } N_{\mu F} > 1/15 \tag{38}$$

where the viscosity number is based upon the Taylor instability wavelength, and is defined as

$$N_{\mu F} = \frac{\mu_F}{(\rho_F \sigma \sqrt{\sigma/g\Delta\rho})^{1/2}} \tag{39}$$

To compare the present data with this criterion, the term j_G was replaced with v_{rel}, or with v_{rel}/α (see Fig. 9). While this latter substitution gives slightly better results, experimental scatter is significant, since for each test run there was a range of gas velocities over which sinuous and roll wave break-up were competing, making it impossible to define a single point as the start of roll wave jet break-up. With roll waves first appearing at the crests of sinuous waves, one might assume that v_{rel}/α would be the correct term to use in place of j_G. Values of α and v_{rel} where corrected to represent those at 1/2 the break-up time (assuming only gravity acceleration) while the initial Re_J values were used for Fig. 9.

For comparison with free jet literature, where atomization has not been established as being due to roll wave entrainment, one can insert "typical" values into Eqs. (37) and (38). For a turbulent water jet issuing into air,

$$v_{J,III} \doteq 16 \text{ m/s} \tag{39}$$

In terms of We_G, a 0.2 cm diameter jet such as Miesse [11] used for much of his data, would result in an atomization criterion of

$$We_{G,III} = 7.7 \tag{40}$$

which is comparable to Miesse's value of 6.35 (Eq. (18)).

3. Jet Surface

Surface conditions were observed for varicose, sinuous, and roll wave break-up, with wavelength/jet diameter plotted against $We_{G,rel}/\alpha^2$ in Fig. 10. All values were corrected to represent conditions at the point of observation, assuming only gravity acceleration.

For varicose break-up there is considerable variation in the data, with an average wavelength of

$$\lambda = 5.2d \quad ; \quad [We_{G,rel}/\alpha^2] < 1.73 \tag{41}$$

which is comparable to Rayleigh's expression (2)

$$\lambda = 4.51\ d \tag{2}$$

while in the drag-induced break-up region wavelength steadily decreases to less than one jet diameter. A rough correlation for this regime would be

$$\lambda = 6.8\ [We_{G,rel}/\alpha^2]^{-0.5}\ d \quad ; \quad [We_{G,rel}/\alpha\ ]^2 > \ 1.73 \tag{42}$$

For low void fractions roll waves were limited in amplitude by the proximity of the pyrex wall. At higher void fractions, however, roll waves were able to grow to large dimensions, sometimes deforming the jet into sheets and ligaments with no discernible cylindrical core (see Fig. 8). This large deformation occurred within the last few jet diameters of jet length.

For higher gas velocities, jets under sinuous break-up no longer had a smooth sinusoidal shape. Wave crests became pointed, and downstream surfaces of each wave were at much steeper slopes than upstream surfaces (see Fig. 7). Such surface distortions were predicted by Filyand [34] using non-linear analysis.4. Dispersed Core Droplet Size

For varicose and sinuous jet break-up, the core is initially dispersed into large liquid slugs. As first suggested by Tyler [35], these slugs should have the same volume as a cylinder of jet diameter and of length equal to the maximum growth rate wavelength. Equations (42) and (43) can be used to give wavelength values for varicose and sinuous jets, respectively, although Fig. 10 shows the great scatter in the data. The subsequent disintegration of these large slugs was not observed in the experiments, due to wall wetting and limited observation length beyond the point of jet break-up. It is assumed that these slugs would disintegrate according to standard droplet break-up mechanisms based on the Weber number criterion, such as

$$We_d = \frac{\rho_G v_G^2 d_{max}}{\sigma} = 8 \sim 17 \qquad (44)$$

which was the estimation of Kataoka et al. [36]. However, at low void fractions the droplet, becoming more spherical beyond the jet break-up point, may expand radially, accelerating the gas flow and perhaps inducing roll wave entrainment. This is similar to the phenomenon observed during the inception of roll waves on the jet core, since these waves first appeared on the crests of sinuous waves.

For roll wave entrainment jet break-up, little droplet size data could be obtained, since roll waves and their entrained droplets wetted the wall after the point of jet break-up, creating an annulus of rough wavy liquid which

obscured the dispersed droplet core. However, a limited number of photographs were obtained in which droplets were observed immediately after being sheared from roll wave crests. From these photographs maximum droplet diameters were measured, within an accuracy of ~0.05 mm. Most droplet diameters were within the range of 0.25-0.55 mm for flows ranging from early roll-wave inception to well established roll wave entrainment break-up of the jet core.

To analyze this limited data, use was again made of roll wave entrainment studies in annular flow. Kataoka et al. [36] related the force balance on a ligament about to be torn from a roll wave crest to the interfacial shear stress in annular two phase flow. Their results predict droplet sizes and size distributions in reasonable agreement (±40%) with various experimental studies. Modifying their droplet size expression to account for geometric differences between annular flow and the present experimental study (v_{rel}/α in place of j_G, gas annulus hydraulic diameter in place of annular flow gas core hydraulic diameter), the average maximum droplet diameter is predicted by

$$d_{max} = 0.088 \frac{\sigma}{\rho_G (v_{rel}/\alpha)^2} Re_J^{-1/6} \left(\frac{Re_{G,rel}}{\alpha}\right)^{2/3} \left(\frac{\rho_G}{\rho_J}\right)^{-1/3} \left(\frac{\mu_G}{\mu_J}\right)^{2/3} \quad (45)$$

with a volume mean diameter equal to $d_{max}/3.13$, according to their droplet size distribution correlation.

This expression was used to predict droplet diameters at the flow conditions of the test trials in which roll wave entrained droplets were actually observed. Conditions were adjusted to represent those at the point of observation. The ratio of observed to predicted droplet diameter was then plotted vs. $[We_{G,rel}/\alpha^2]$ in Fig. 11. Although the number of data points is limited, and the concept of average maximum diameter becomes vague when only a few droplets are observed at each data point, the results show general

agreement in the high gas velocity region (small predicted diameters). Agreement is not as good for lower gas velocities (larger predicted diameters).

The velocity dependence of $v_{rel}^{-4/3}$ indicated by Eq. (45) is quite close to the v_{rel}^{-1} dependence indicated for free jets by Eqs. (21) and (22). However, these latter equations show liquid viscosity and density dependence opposite that of Eq. (45). For typical test conditions, Eq. (22) predicts droplet sizes similar to those observed, while Eq. (21) yields slightly larger droplet sizes.

The failure of Eq. (45) to predict the observed maximum droplet sizes in the sinuous-to-roll wave transition regime, and in the beginning of the roll wave regime itself, might be explained by examining the geometry at the point of droplet formation. At high relative velocities, well into the roll wave regime, droplets are forming at the wave crests before the roll wave itself extends far beyond the jet surface and into close proximity with the pyrex wall. Droplets formed in this manner have relatively large free paths and flight times, before they can approach the pyrex wall and possibly be deposited in the annular liquid film forming there. On the other hand, at lower relative velocities, longer jet break-up times allow the core bulk motion to become, to varying degrees, somewhat sinuous. Maximum roll wave growth occurs on the crests of these sinuous waves, and the roll waves themselves are still relatively small when brought into close proximity with the pyrex wall by bulk core motion. The mean free path of droplets at this point of formation is much smaller than in the previous case, and droplet deposition occurs more rapidly. This is especially true for the larger droplets, which are accelerated beyond the wave crests, and into the larger flow areas between crests, less rapidly than smaller droplets. And so, for

our adiabatic test section, it becomes very unlikely that the larger droplets formed at this point will be observed.

In an attempt to observe dispersed core droplet size beyond the point of wall wetting and the inception of rough wavy annular flow, a limited number of trials were run on a shortened test section. The end of the pyrex tube was flared outward, and a concentric cone was placed inside this flare to divert the liquid annular flow away from the test section exit. Photographs were taken at the exit, with the distance between jet break-up and section exit varied.

Results were obtained at several flow conditions within the roll wave entrainment regime. At points near the jet break-up length, large droplets and ligaments from the distorted jet core, created when roll waves expanded to the pyrex wall, were observed. These larger dispersed liquid masses continued to break-up beyond the jet break-up point, so that at a distance approximately two jet lengths from the jet nozzle exit, only dispersed droplets appeared. These droplets could be divided into two size groups, one with diameters of 0.2-0.7 mm, and a second with diameters near 2-3 mm. The first group is of the same general size as droplets observed to form from roll waves. The second group may represent break-up of the remnants of the jet core, perhaps based on a Weber number criterion such as Eq. (44). Equation (44), however, predicts droplet sizes of approximately 4-12 mm for the test conditions.

A second break-up mechanism for these larger droplets can be postulated by considering a study on wake regime flow by Kataoka and Ishii [37]. This study gives an expression for maximum stable drop

$$d_{max} = 4\sqrt{2}\sqrt{\frac{\sigma}{g\Delta\rho}}N_{\mu G}^{1/3} \tag{46}$$

where the gas viscosity number is based on the Taylor instability wavelength, and is defined as

$$N_{\mu G} = \frac{\mu_G}{(\rho_G \sigma \sqrt{\sigma/g\Delta\rho})^{1/2}} \tag{47}$$

For these limited test conditions Eq. (46) predicts a maximum droplet size of approximately 1.6 mm, an improvement over the sizes predicted by Eq. (44).

Results from this limited number of trials using the shortened test section are not conclusive, since only a small amount of data was obtained. In addition, the effectiveness of the liquid annular film diverter has not been established, so that some of the observed droplets may have been formed at the diverter itself. And finally, the effect of wall wetting makes any observations beyond the point of jet break-up suspect when applying them to actual inverted annular flow, where such wetting does not occur.

To compare dispersed droplet size data obtained in this experiment with actual inverted annular flow is difficult, since most low quality film boiling experiments do not produce such data. An exception is the PWR FLECHT SEASET series of experiments, in which heated rod bundles are quenched by water, at pressures up to 0.41 MPa. In a report by Lee et al. [38], dispersed droplet sizes and velocities are examined at various distances above the quench front. Most of the droplets are in the range of 0.5 to 1.5 mm, with velocities from 1 m/s up to 12 m/s. Smaller droplets, however, may have been overlooked in these experiments, due to relatively long exposure times for their photography (motion picture cameras at speeds up to 2500 frames per second). At their shortest exposure time, ~160 μs, a droplet 1 mm in diameter, moving at 6 m/s would travel a distance equal to its diameter during the exposure. Much smaller droplets, or ones at higher velocities, would be

seen, at best, as poorly defined blurs. In contrast, the 3 μs exposure time used in our experiments would have similar resolution for a 0.1 mm drop with velocities up to 30 m/s.

CONCLUSIONS

For these experiments, adiabatically simulating inverted annular flow with turbulent water jets and various gas annuli, the data can be presented in the following manner:

(1) By extending free jet studies to these coaxial jets (introducing the gas Weber number based on relative velocity and the void fraction), break-up length data in the varicose regime can be correlated by

$$L/d = 481\ [Re_J]^{-0.5306}\ \sqrt{We_J} \quad ; \quad \text{for } [We_{G,rel}/\alpha^2] < 1.73$$

and, in the sinuous and roll wave regimes, by

$$L/d = 687\ [Re_J]^{-0.5306}\ \sqrt{We_J}\ [We_{G,rel}/\alpha^2]^{-0.6467} \quad ;$$

$$\text{for } [We_{G,rel}/\alpha^2] > 1.73$$

with data scatter only significant for the first correlation, and in transition region near $[We_{G,rel}/\alpha^2] = 1.73$.

(2) Jet break-up mechanisms were identified and correlated. For the transition from varicose jet break-up to sinuous jet break-up, a criterion similar to that for free jets was developed,

$$[We_{G,rel}/\alpha^2] > 1.73$$

while the transition from sinuous break-up to roll wave entrainment break-up was correlated well by modifying a criterion for annular rough turbulent flow into the following:

$$\frac{\mu_J(v_{rel}/\alpha)}{\sigma}\sqrt{\frac{\rho_G}{\rho_J}} > N_{\mu F}^{0.8} \quad ; \quad \text{for } N_{\mu F} < 1/15$$

(3) Jet surface conditions were observed and the following rough correlations for maximum growth rate wavelength were developed:

$$\lambda = 5.2\ d \quad ; \quad \text{for } [We_{G,rel}/\alpha^2] < 1.73$$

$$\lambda = 6.8\ [We_{G,rel}/\alpha^2]^{-0.5}\ d \quad ; \quad \text{for } [We_{G,rel}/\alpha^2] > 1.73$$

The deformation of sinuous and roll waves was noted and described.

(4) Dispersed core droplets formed at roll wave crests were observed. For those formed at high gas velocities, where the largest droplets still have appreciable flight time before deposition, limited droplet diameter data was correlated well by modifying an expression developed for annular flow into the following form:

$$d_{max} = 0.088\ \frac{\sigma}{\rho_G(v_{rel}/\alpha)^2}\ Re_J^{-1/6}\left(\frac{Re_{G,rel}}{\alpha}\right)^{2/3}\left(\frac{\rho_G}{\rho_J}\right)^{-1/3}\left(\frac{\mu_G}{\mu_J}\right)^{2/3}$$

Other droplet formation mechanisms may become important after the jet core is disrupted by large amplitude roll waves. However, no conclusive data was obtained to identify such mechanisms as may have produced the 2-3 mm droplets observed beyond core disruption.

For sinuous and varicose jet break-up, the size of the liquid slugs resulting from the break-up may be estimated from the wavelength correlations presented. Subsequent break-up of these slugs could not be observed with our test system.

Due to wall wetting, observations made at or beyond the point of jet break-up may not be applicable in the case of actual inverted annular flow. In addition, the experimental study has been limited, by the physical constraints of test section construction, to void fractions no lower than 0.28. As a result, the correlations developed here may not be applicable at very low void fractions, where the term v_{rel}/α becomes very large.

ACKNOWLEDGMENTS

This work was performed at Argonne National Laboratory, under the auspices of the U.S. Nuclear Regulatory Commission.

We would like to thank Drs. N. Zuber and M. Young of the NRC for their guidance and assistance in this research, and to thank G. Lambert, E. Sowa and A. Tokuhiro of ANL for help in constructing the experimental apparatus.

REFERENCES

1. Weber, C., "Zum Zerfall eines Flussigkeitsstrahles," Z. Angew. Math. Mech., Vol. 11, 1931, p. 136.

2. Lord Rayleigh, "On the Instability of Jets," Proc. Lond. Math. Soc., Vol. 10, 1878, p. 4.

3. Lafrance, P., "Nonlinear Breakup of a Liquid Jet," Phys. Fluids, Vol. 17, 1974, p. 1913.

4. Christiansen, R. M. and Hixson, A. N., "Breakup of a Liquid Jet in a Denser Liquid," Ind. Eng. Chem., Vol. 49, 1957, p. 1017.

5. Tyler, E. and Watkin, F., "Experiments with Capillary Jets," Phil. Mag., Vol. 14, 1932, p. 849.

6. Grant, R. P. and Middleman, S., "Newtonian Jet Stability," AIChE J., Vol. 12, 1966, p. 669.

7. McCarthy, M. J. and Molloy, N. A., "Review of Stability of Liquid Jets and the Influence of Nozzle Design," Chem. Eng. J., Vol. 7, 1974, p. 1.

8. Phinney, R. E., "Stability of a Laminar Viscous Jet - The Influence of the Initial Disturbance Level," AIChE J., Vol. 18, 1972, p. 432.

9. Fenn, R. W. and Middleman, S., "Newtonian Jet Stability: The Role of Air Resistance," AIChE J., Vol. 15, 1969, p. 379.

10. Smith, S. W. J. and Moss, H., "Experiments with Mercury Jets," Proc. Roy. Soc., Vol. A-93, 1917, p. 373.

11. Miesse, C. C., "Correlation of Experimental Data on the Disintegration of Liquid Jets," Ind. Eng. Chem., Vol. 47, 1955, p. 1690.

12. Chen, T.-F. and Davis, J. R., "Disintegration of a Turbulent Water Jet," Proc. ASCE, Hyd. Div., Vol. 90, 1964, p. 175.

13. Litlaye, G., _____, Pub. Sci. Tech. Secret. Aviation, 1942, as cited in Ref. 7.

14. Iciek, J., "The Hydrodynamics of a Free, Liquid Jet and Their Influence on Direct Contact Heat Transfer - II," Int. J. Multiphase Flow, Vol. 8, 1982, p. 251.

15. Tyler, E. and Richardson, E. G., "The Characteristic Curves of Liquid Jets," Proc. Phys. Soc., Vol. 37, 1925, p. 297.

16. Iciek, J., "The Hydrodynamics of a Free, Liquid Jet and Their Influence on Direct Contact Heat Transfer - I," Int. J. Multiphase Flow, Vol. 8, 1982, p. 239.

17. Baron, T., _____, Tech. Rept. Univ. Illinois No. 4, 1949, as cited in Ref. 11.

18. Phinney, R. E., "Breakup of a Turbulent Liquid Jet in a Low Pressure Atmosphere," AIChE J., Vol. 21, 1975, p. 996.

19. van de Sande, E. and Smith, J. M., "Jet Break-up and Air Entrainment by Low Velocity Turbulent Water Jets," Chem. Eng. Sci., Vol. 31, 1976, p. 219.

20. Ohnesorge, W., "Die Bildung von Tropfen an Dusen und die Anflosung flussiger Strahlen," Z. Angew Math. Mech., Vol. 16, 1936, p. 355.

21. Brodkey, R. S., "The Phenomena of Fluid Motion," Addison-Wesley, Reading, MA (1967).

22. LiHaye, G., _____, Compt. rend., Vol. 217, 1943, p. 99, as cited in Ref. 11.

23. Merrington, A. C. and Richardson, E. G., "The Break-up of Liquid Jets," Proc. Phys. Soc., Vol. 59, 1947, p. 1.

24. Levich, V. G., "Physicochemical Hydrodynamics," Prentice-Hall, NY (1962).

25. Tanazawa, Y. and Toyoda, S., _____, Trans. JSME, Vol. 20, 1954, p. 306, as cited in Ref. 7.

26. Lienhard, J. H. and Day, J. B., "The Breakup of Superheated Liquid Jets," J. Basic Eng. Trans. ASME, Vol. 92, 1970, p. 515.

27. Kusui, T., "Liquid Jet Flow into Still Gas," JSME Bulletin 5, Vol. 11, 1968, p. 1084.

28. Ivanou, V. A., "Disintegration of a Liquid Jet," J. Appl. Mech. Tech. Phys. USSR, Vol. 7, 1966, p. 19.

29. Nukiyama, S. and Tanasawa, Y., "Experiment on Atomization of Liquid," Trans. JSME, Vol. 5, 1939, p. 63.

30. Jensen, R. T., "Ineception of Liquid Entrainment During Emergency Cooling of Pressurized Water Reactors," Ph.D. Thesis, Utah State University, 1972.

31. Cunningham, R. G. and Doplin, R. J., "Jet Breakup and Mixing Throat Lengths for the Liquid Jet Gas Pump," J. Fluids Eng. Trans. ASME, Vol. 96, 1974, p. 216.

32. Wallis, G. B., "One Dimensional Two-phase Flow," McGraw-Hill, NY (1969).

33. Ishii, M. and Grolmes, M. A., "Inception Criteria for Droplet Entrainment in Two-Phase Cocurrent Film Flow," AIChE J., Vol. 21, 1975, p. 308.

34. Filyand, L. V., "Instability and Breakup of Capillary Liquid Jets in a Parallel Airstream," Fluid Dynamics, Vol. 16, 1981, p. 424.

35. Tyler, E., "Instability of Liquid Jets," Phil. Mag., Vol. 16, 1933, p. 504.

36. Kataoka, I., Ishii, M. and Mishima, K., "Generation and Size Distribution of Droplet in Annular Two-Phase Flow," to be published in J. Fluid Eng. Trans. ASME, 1983.

37. Kataoka, I. and Ishii, M., "Mechanism and Correlation of Droplet Entrainment and Deposition in Annular Two-Phase Flow," ANL-82-44, NUREG/CR-2885 (1982).

38. Lee, N., Wong, S., Yeh, H. C. and Hochreiter, L. E., "PWR FLECHT SEASET Unb'ocked Bundle, Forced and Gravity Reflood Task Data Evaluation and Analysis Report, NRC/EPRI/Westinghouse Report No. 10," NUREG/CR-2256, EPRI NP-2013, WCAP-9891 (1981).

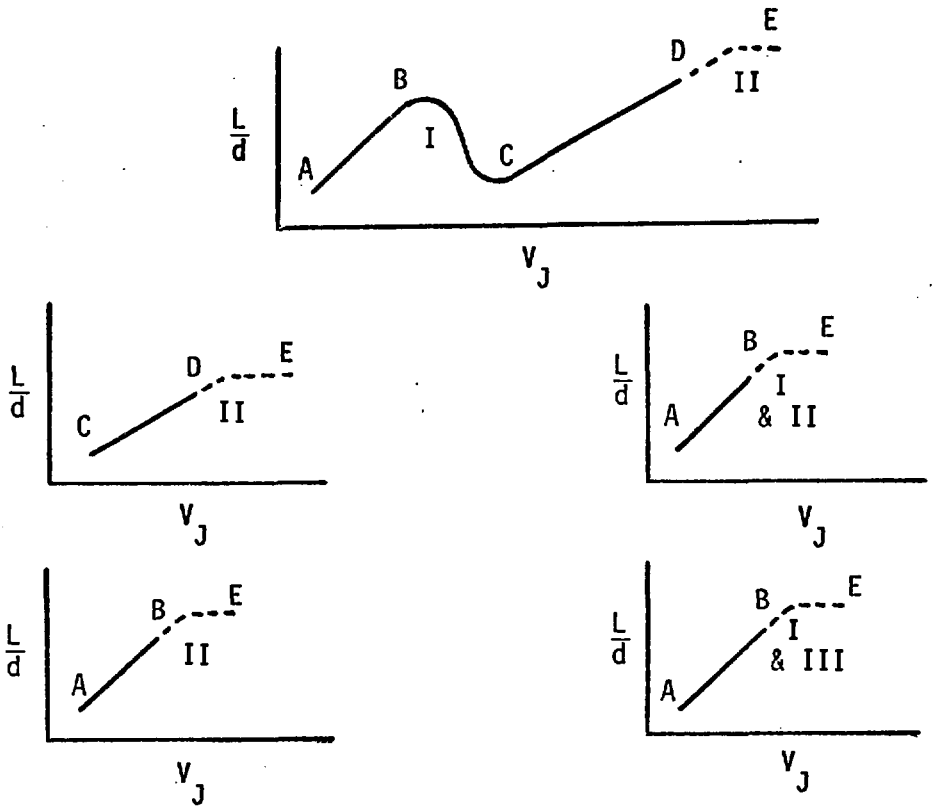

FIG. 1 POSSIBLE BEHAVIOR, FREE JET

AB Laminar, varicose
CD Turbulent, varicose
E Drag-induced break-up

I Transition, laminar/turbulent
II Transition, varicose/sinuous
III Transition, sinuous/atomization or varicose/atomization

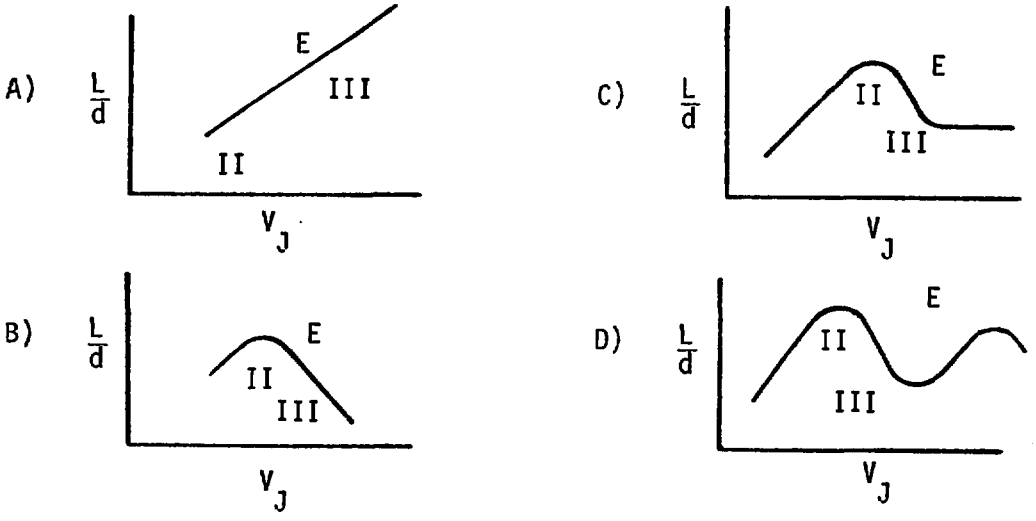

FIG. 2 POSSIBLE DRAG-INDUCED BREAK-UP BEHAVIOR, FREE JET

A) Tanazaw and Toyoda, etc.
B) Lienhard and Day, etc.
C) Kusui
D) Ivanov

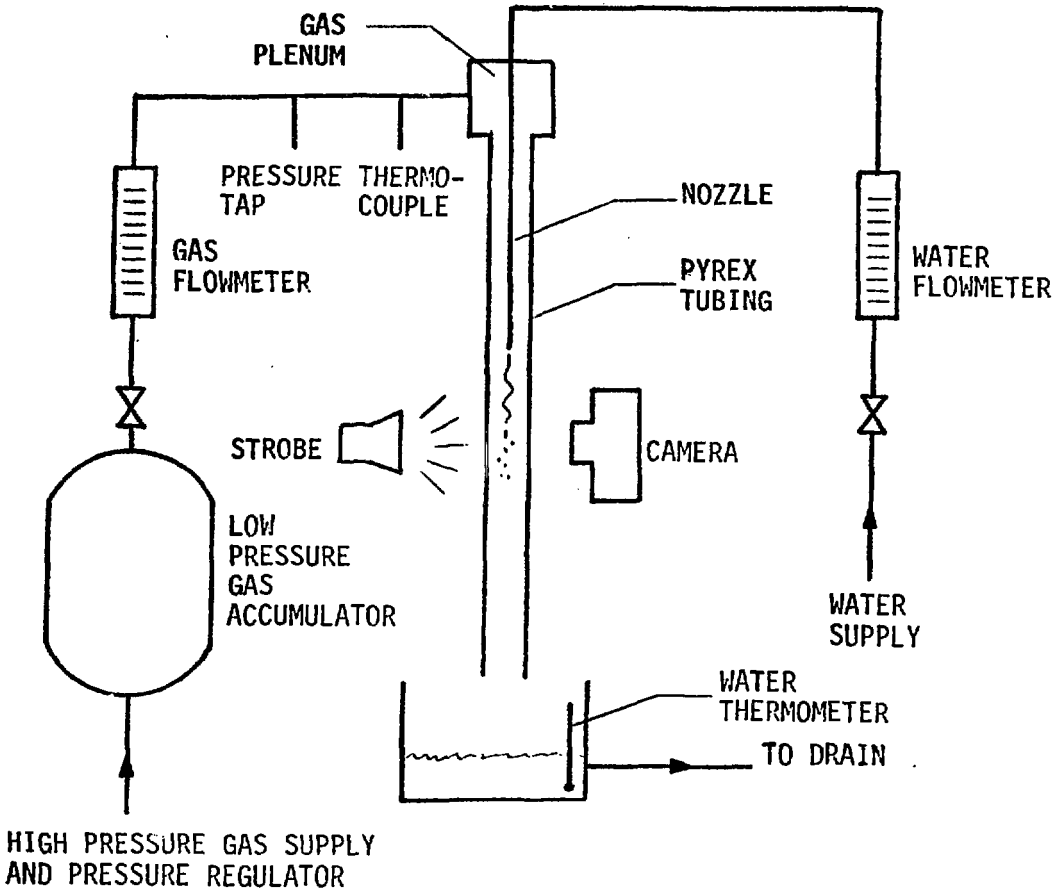

FIG. 3 SCHEMATIC DIAGRAM OF TEST SYSTEM

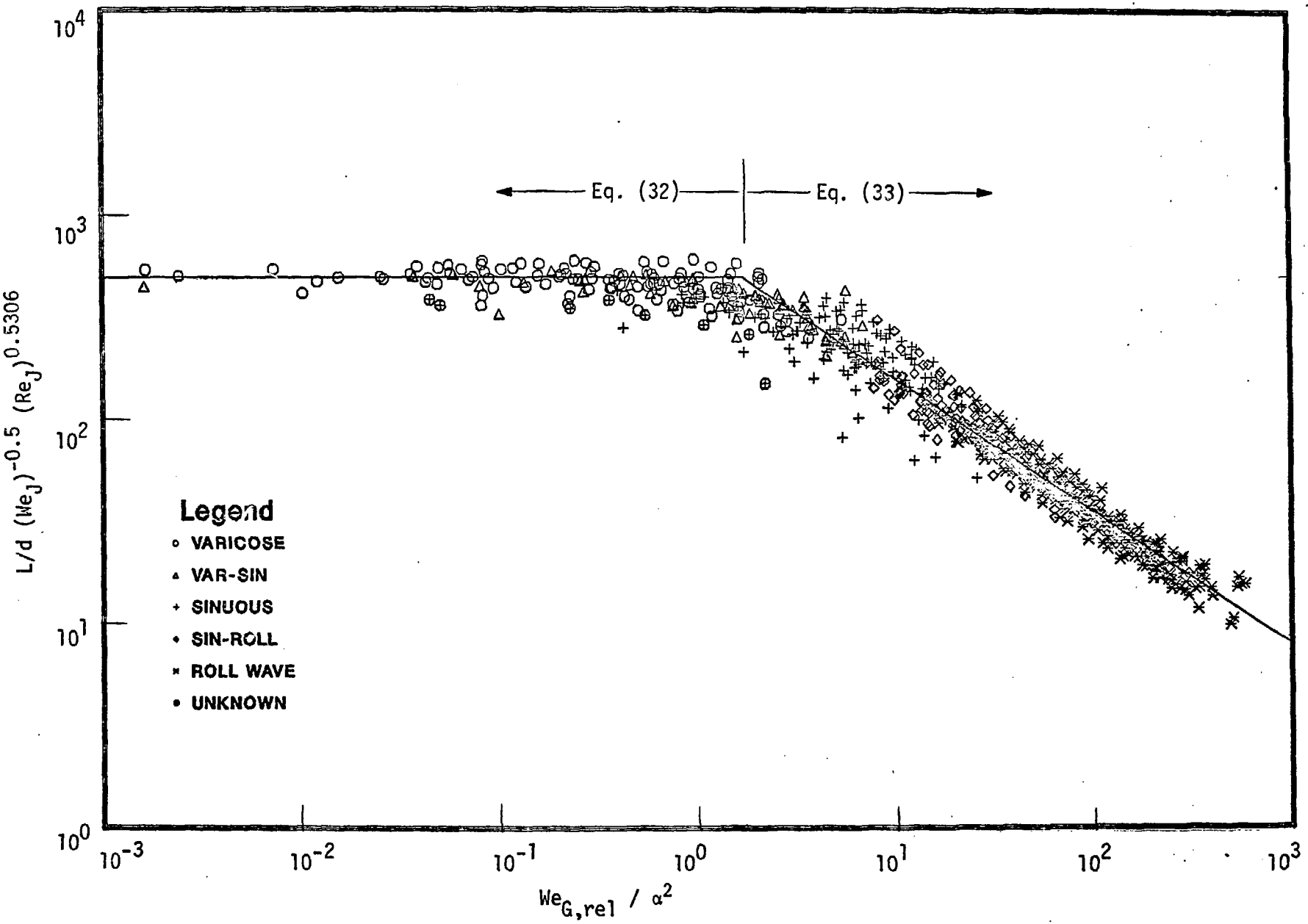

FIG. 4 CORRELATION OF BREAK-UP LENGTH DATA, WITH BREAK-UP MECHANISMS

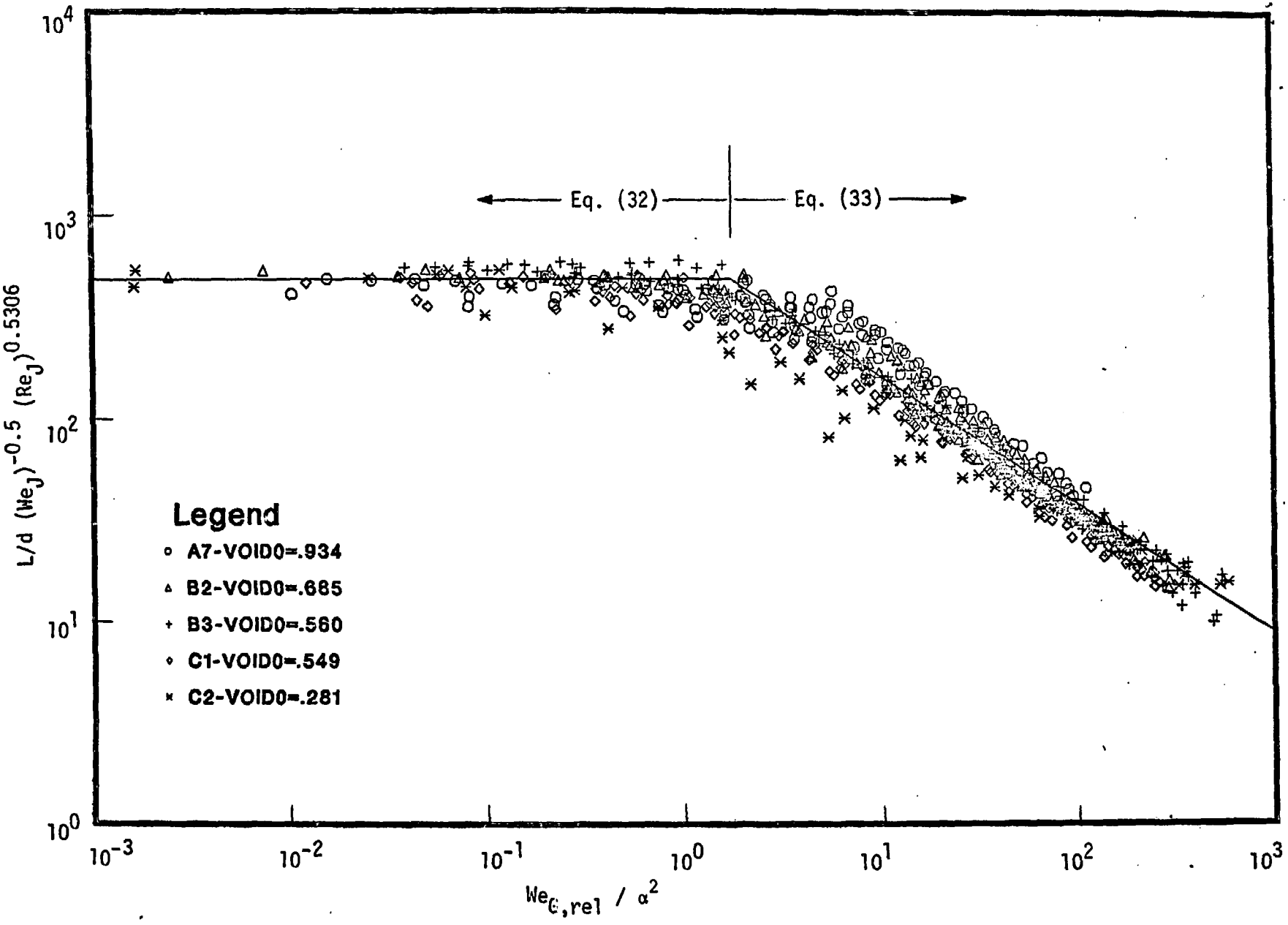

FIG. 5 CORRELATION OF BREAK-UP LENGTH DATA, WITH INITIAL VOID FRACTIONS

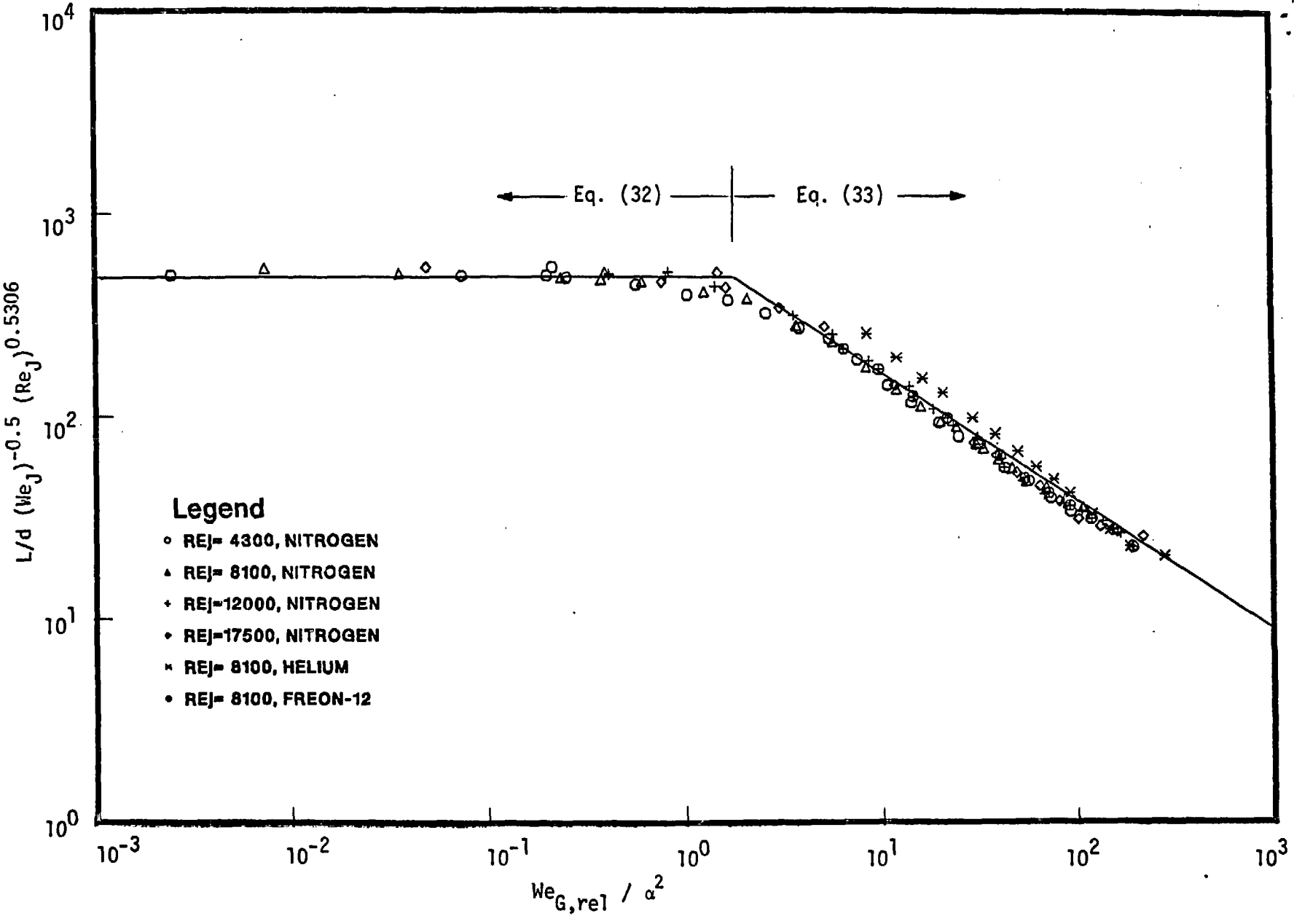

FIG. 6 CORRELATION OF BREAK-UP LENGTH DATA, WITH Re_J AND GAS DENSITY (B2 TEST SERIES)

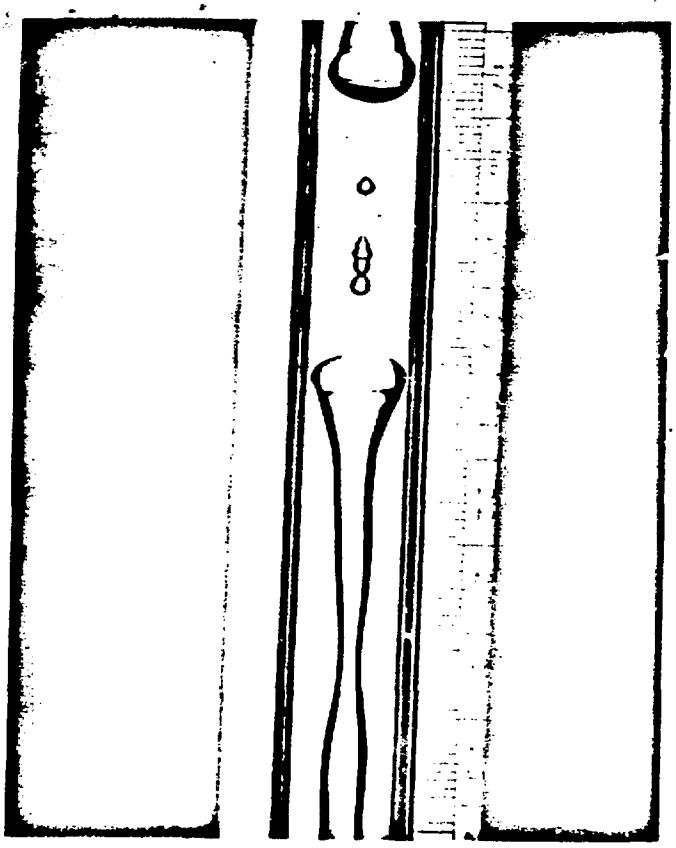

(A)

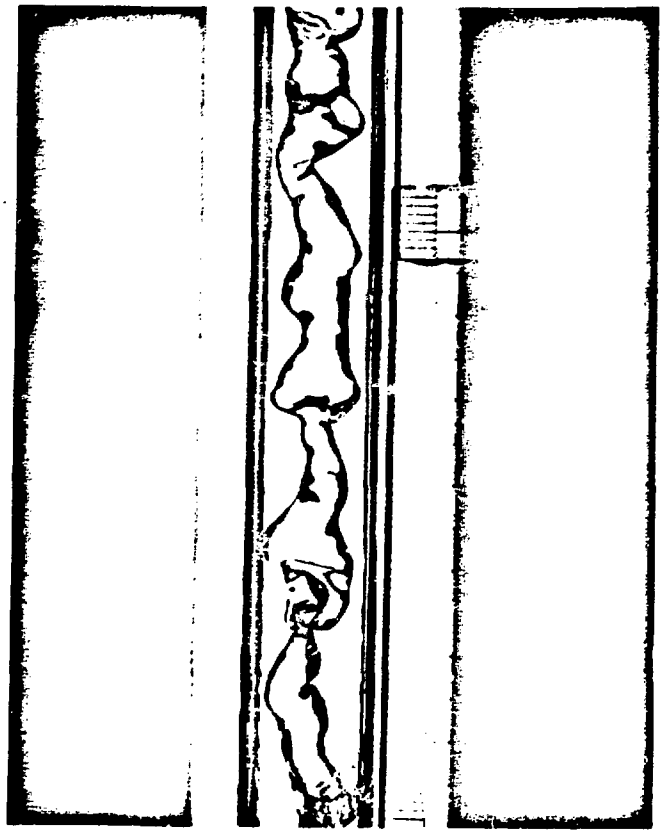

(B)

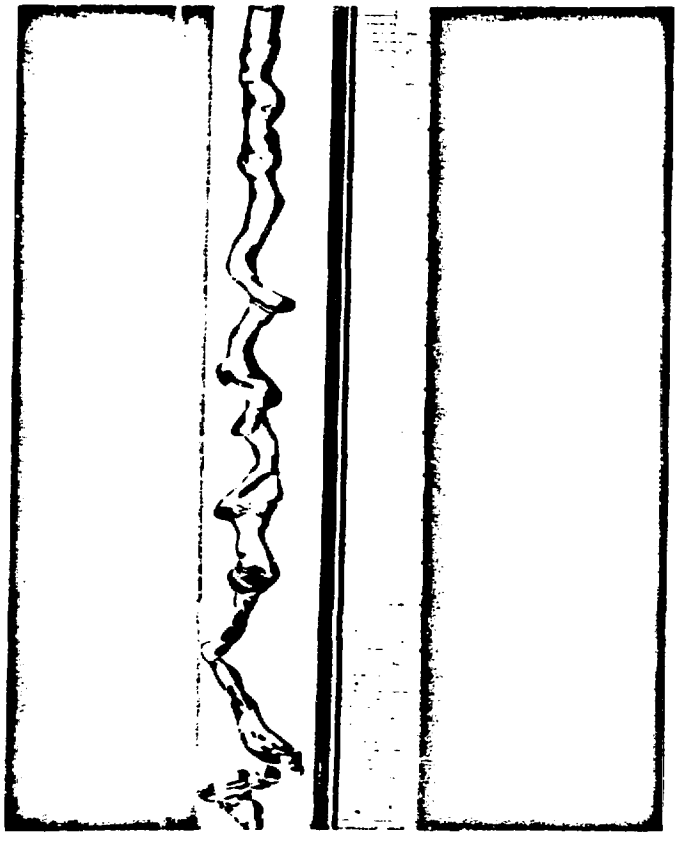

(C)

FIG. 7 VARICOSE AND SINUOUS JET BREAK-UP PHOTOGRAPHS

(A) Varicose break-up, low degree of turbulence, satellite droplets

(B) Sinuous break-up, significant turbulence, waves distorted from sinusoidal shape by gas flow

(C) Sinuous break-up, high void fraction, large wave amplitude before break-up

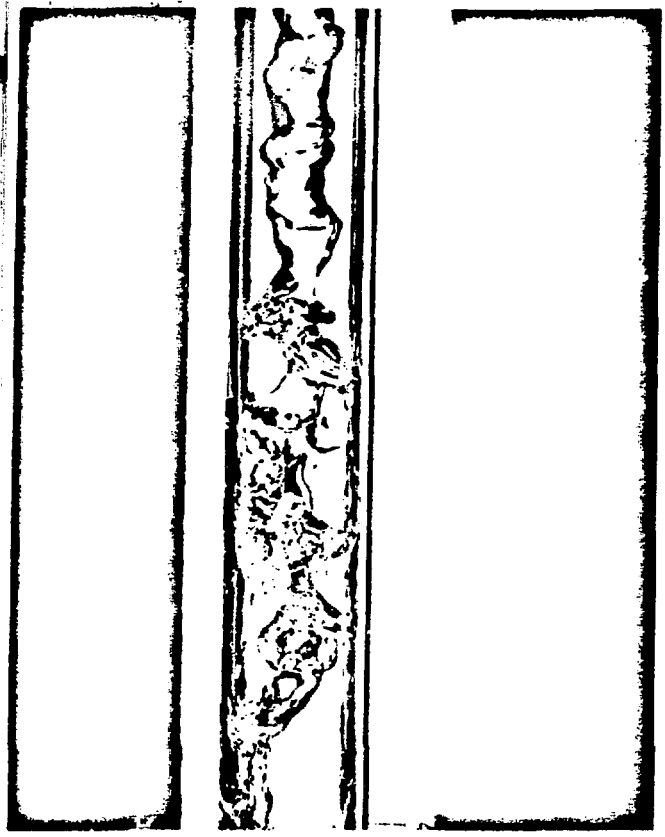

(A)

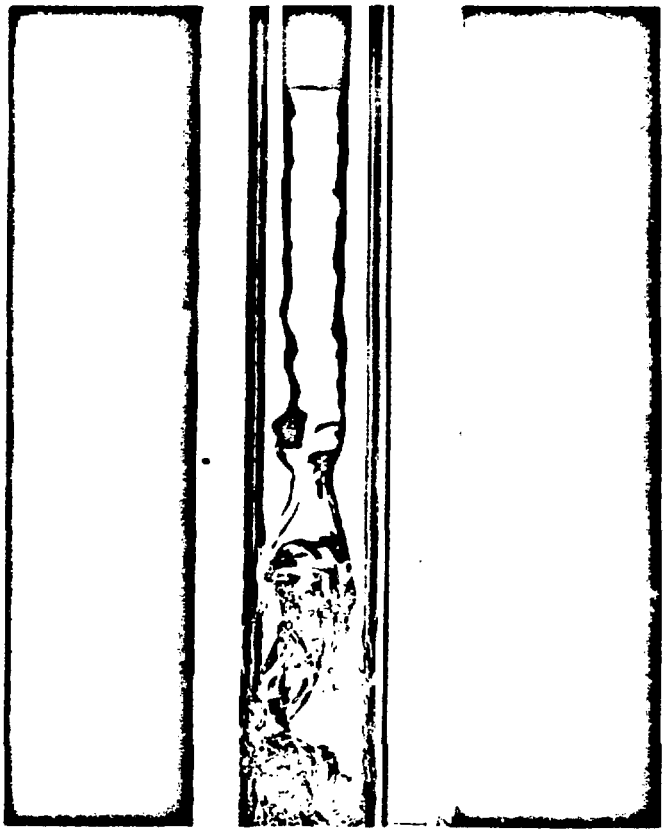

(B)

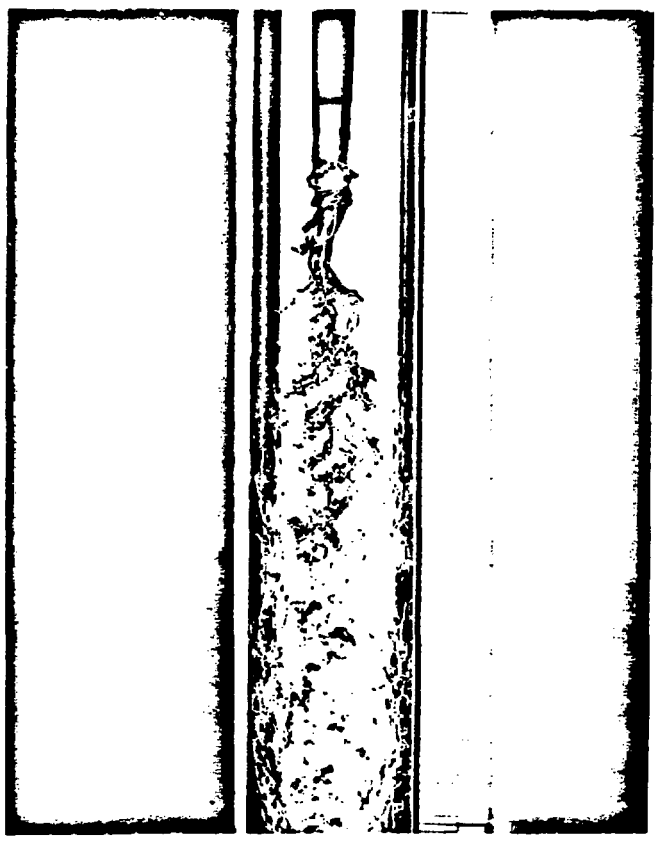

(C)

FIG. 8 ROLL WAVE INCEPTION/ENTRAINMENT JET BREAK-UP PHOTOGRAPHS

(A) Sinuous-roll wave jet break-up transition, roll waves form at sinuous wave crests, significant turbulence

(B) Roll wave entrainment break-up, droplets sheared from roll wave crest

(C) Roll wave break-up, high void fraction, large amplitude waves distort core into sheets and ligaments

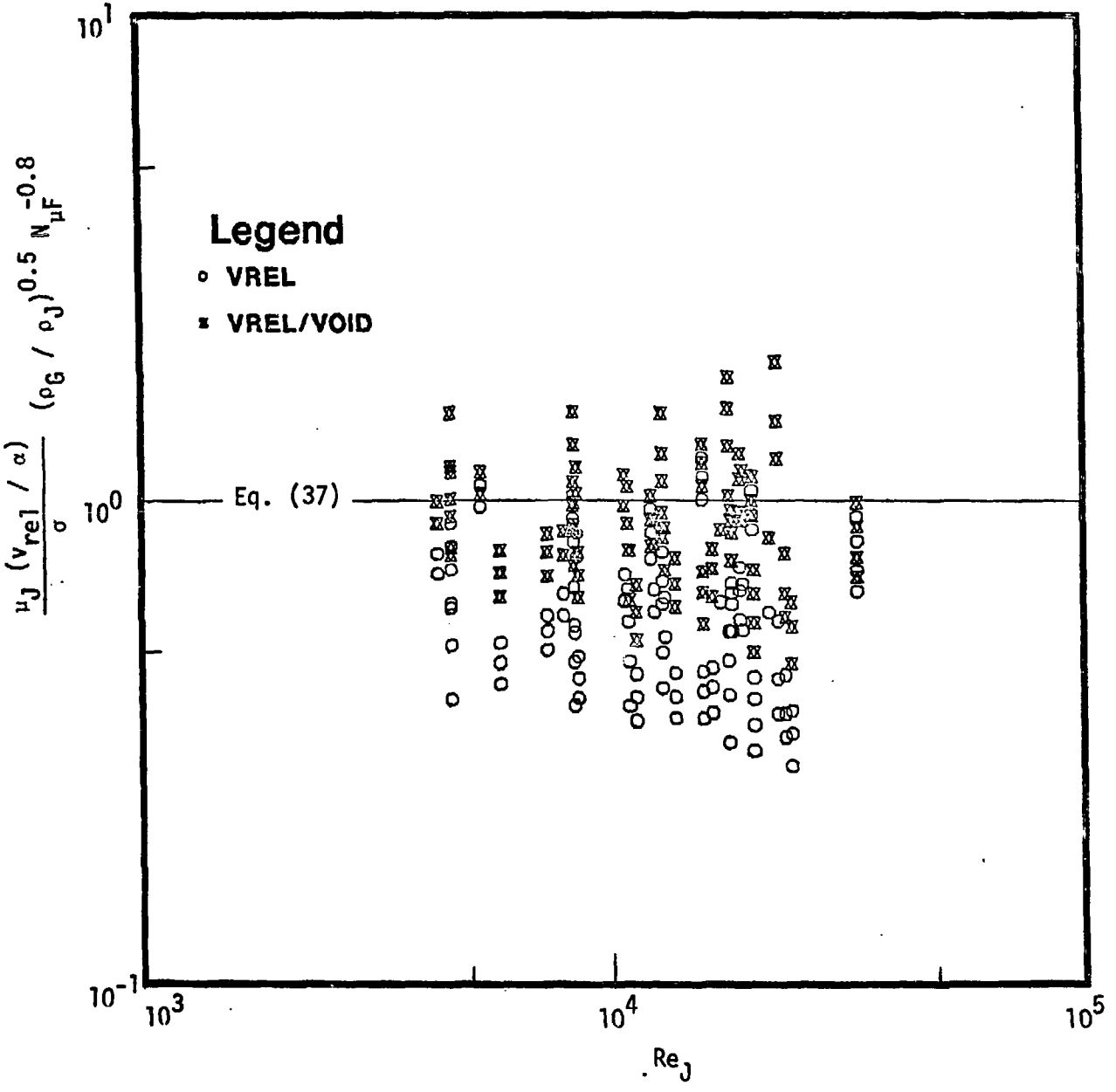

FIG. 9 CORRELATION OF ROLL WAVE ENTRAINMENT INCEPTION DATA

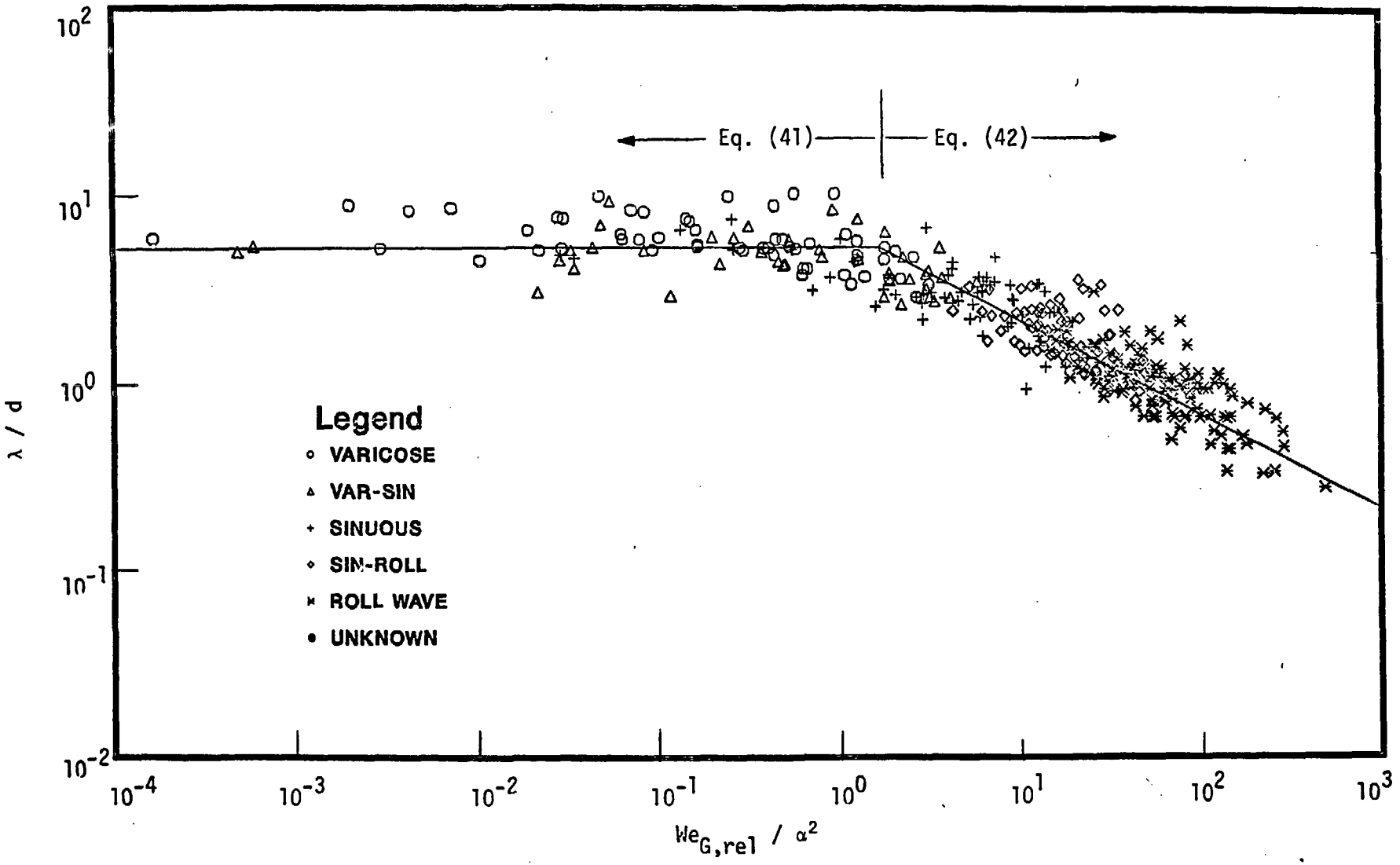

FIG. 10 CORRELATION OF WAVELENGTH DATA

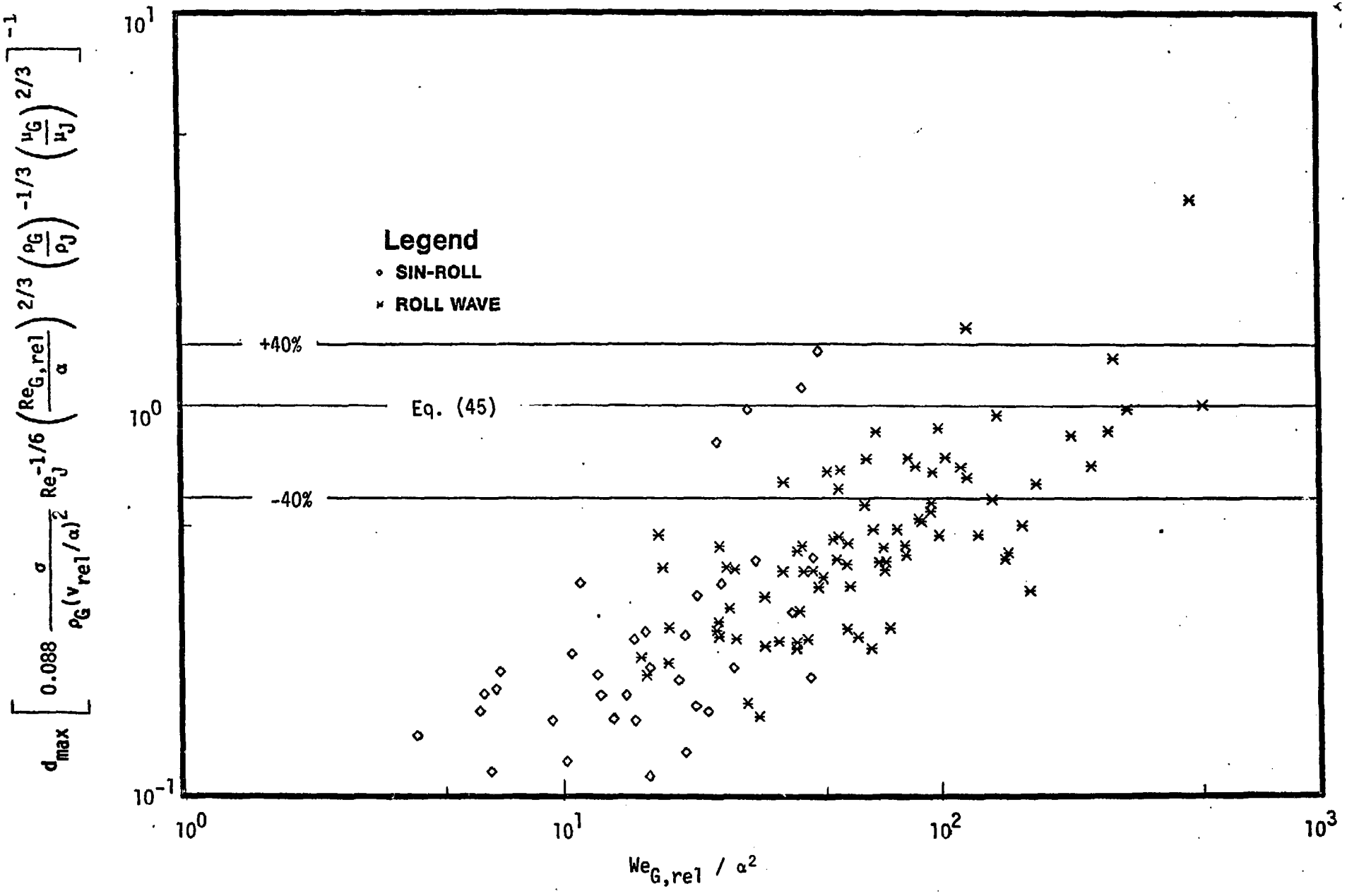

FIG. 11 CORRELATION OF ROLL WAVE ENTRAINMENT DROPLET SIZE DATA